



An automatic device for *in vivo* absorption spectra acquisition and chlorophyll estimation in phytoplankton cultures

Emilie Le Floc'h, Gilbert Malara & Antoine Sciandra*

Laboratoire d'Océanographie de Villefranche, Université Pierre et Marie Curie and CNRS, UMR 7093, BP 28, 06234 Villefranche sur Mer CEDEX, France; *Author for correspondence (phone +33-(0)4-9376-3819; fax +33-(0)4-9376-3834; e-mail sciandra@obs-vlfr.fr)

Received 20 September 2001; revised 8 April 2002; accepted 30 April 2002

Key words: Automatic culture system, Chemostat, Chlorophyll *a*, Cryptophyceae, *In vivo* absorption, Nitrogen limitation, Packaging effect, Phycoerythrin, *Rhodomonas salina*

Abstract

In order to aid the study of photoacclimation, a new programmable device is described which provides automatic on-line acquisition of *in vivo* cell absorption in phytoplankton cultures. The system was used for a long-term study of *Rhodomonas salina* grown at constant photon flux density in a nitrate-limited continuous culture with different dilution rates. Particulate absorption measured at the red chlorophyll *a* (Chl *a*) maximum was not a good proxy of biomass, because of the large variability of cellular chlorophyll induced by nitrogen limitation. However, the device is well suited to automatic assessment of Chl *a* and phycoerythrin (PE) concentrations in phytoplankton cultures, if algal cell size and concentration are measured in parallel to correct the packaging effect. The effects of nitrogen limitation on Chl *a* and PE contents and particle absorbance are discussed.

Introduction

Cells adapt to changes in PAR by modifying their absorption efficiency to photosynthetic energy requirements (Dubinsky 1992). Variations in photon flux intensity and spectrum modify the concentration (photoacclimation) and composition (chromatic adaptation) of pigments, respectively. Their integrated effects are reflected in the variation in the PI curve parameters obtained at different growth intensities (Anning et al. 2000). One of the most studied parameters in photoacclimation is light intensity, specially its effects on cell chlorophyll. A smaller number of studies have been reported on the consequences of limiting micro- or macro-nutrients. The effects of dissolved inorganic nitrogen limitation on photoacclimation have been studied more often (Berges et al. 1996; Goericke and Montoya 1998), because N availability often controls oceanic primary productivity.

In view of the structural and functional metabolic interactions between C and N (Turpin 1991), the capacity of cells to adapt to suboptimal light conditions

may depend upon their nitrogen status. Important quantities of nitrogen are mobilized during apoprotein synthesis associated with chlorophyll complexes, as is also the case with Rubisco enzymes, both of which are implicated in light and dark photosynthesis reactions. In cryptophytes, it has been suggested that PE can play the double role as an accessory pigment and nitrogen reservoir (Kana et al. 1992; Sciandra et al. 2000). As a consequence, it seems that lack of nitrogen can hinder both photo- and chromatic adaptation.

Studies in chemostat cultures have shown that the maintenance of optimal growth under a reduced light regime induces additional nitrogen requirement (Rhee and Gotham 1981; Healy 1985) the so-called 'compensation phenomenon'. However, the readjustment of different interacting molecular pathways faced with light and nutritive variations is a non-linear process and is difficult to model. Mathematical models of colimitation generally use either a 'minimal' or 'multiplicative' function. Neither have been verified experimentally, so the exclusive use of either hypothesis is questionable (Sciandra et al. 1997). More

complex models which take into account internal C, N and Chl *a* have been proposed (Geider et al. 1998; Flynn et al. 2001; Pawlowski et al. in press).

The effects of light and nitrogen on photoacclimation also vary in response to hydrodynamic and atmospheric perturbations occurring on a large temporal scale, which complicate the interpretation of data acquired *in situ*. In contrast, responses of organisms adapting to variations in light and nutrients provide data in controlled laboratory conditions, which can validate photoacclimation models. Continuous cultures can combine the effects of light and nutrient limitation, thus providing insights into algal colimitation studies, and especially pigment adaptation. Cells can respond very rapidly to external perturbations, but photoacclimation can be completely achieved after prolonged time, therefore, autonomous devices are necessary to insure suitable sampling of the major variables. With advances in microprocessor technology, data collection can be routinely managed by automatic systems which reduce sampling bias and data noise.

The aim of this paper is to present a device which insures automatic acquisition of *in vivo* spectral absorption in continuous cultures of phytoplankton.

Materials and methods

Experimental design

The Cryptophyceae *Rhodomonas salina* (CCMP1319, Bigelow Laboratory for Ocean Sciences) was grown in continuous culture using an automatic system described by Malara and Sciandra (1991) and Bernard et al. (1996). Details for the vessel preparation, medium preparation, temperature regulation, mixing, bubbling and illumination are given in Stramski et al. (2002). The temperature was maintained at 19 ± 0.1 °C. The nitrate concentration $[\text{NO}_3]$ in the fresh medium (without silicate) was $96 \pm 14 \mu\text{mol L}^{-1}$. The photosynthetically available radiation (PAR, irradiance integrated between 400 and 700 nm) was $93 \pm 11 \mu\text{mol photon m}^{-2} \text{ s}^{-1}$.

Automated acquisition of phytoplankton spectral absorption

The whole culture system ensured frequent and automatic acquisitions of cell size and number, nitrate and nitrite measurements and *in vivo* spectral absorption. Details for the optical particle counter HIAC (Pacific

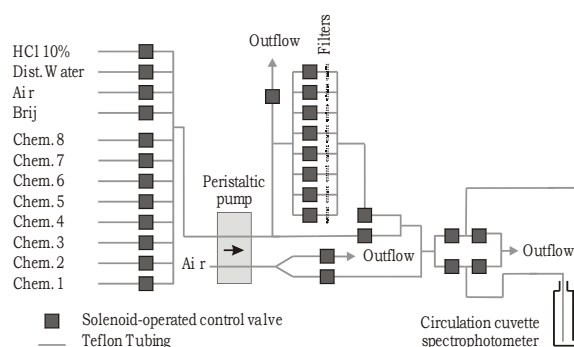


Figure 1. Automatic device for measurement of *in vivo* phytoplankton absorption: schematic representation of the flow circuit between the chemostat cultures (Chem. 1 to 8), rinsing solutions (diluted acid, distilled water, Brij detergent, filtered air) and spectrophotometer cuvette.

Scientific) and autoanalyzer Technicon are given in Bernard et al. (1996). The automation for the spectral *in vivo* absorption acquisition comprises a PC with two interface cards (PCI-20087W-1 and PCI-20428W-2; Intelligent Instrumentation), a UV/visible spectrophotometer (Varian, DMS100), a peristaltic pump (Gilson), a filtration bench (8 Millipore Swinex, Gelman Filter Type A/E 13 mm), 21 simple and 4 double electric valves, and Teflon tubing. Figure 1 shows the flow circulation between the chemostats, the different rinsing solutions and the spectrophotometer flow cuvette.

Sampling preparation. Software developed in Turbo-Pascal controls the sequential execution of discrete steps: rinsing of the overall circuit with different solutions before (Brij detergent, distilled water, filtered culture or culture) and after (HCl 10%, distilled water) spectral acquisition, filtration of culture for blank absorption acquisition, filling, emptying and rinsing of the spectrophotometer cuvette, monitoring of the spectrophotometer for absorption scanning, and data storage. Eight phytoplankton cultures can be sequentially sampled. The length of time required for different steps, and the number of blanks and culture replicates can all be programmed within the software, depending on the species cultured and the required precision. A typical sequence performed during one measurement cycle requires around 29 minutes and uses 100 mL culture (Table 1).

Spectral scanning. The spectral absorption coefficient $a(\lambda)$ was automatically measured on cell suspensions in a 1-cm flow-through quartz cuvette with a

Table 1. Chronological sequence of operations performed during one typical automatic absorption measurement cycle

Operations	Operation sequence			Operation length (s)	
	Rinsing	Scanning cycles			Rinsing
		Reference	Culture		
Air draining	•••	••	••••	20 (×11)	
Filtered culture		•••		60 (× 3)	
Direct culture			••••	60 (× 4)	
Absorption Scan		••	•••	180 (× 5)	
Detergent (Brij 1%)	•			50 (× 1)	
Distilled water	•			60 (× 2)	
Acid (HCl 10%)				50 (× 1)	
Full cycle >			1760 (29.3 min)	

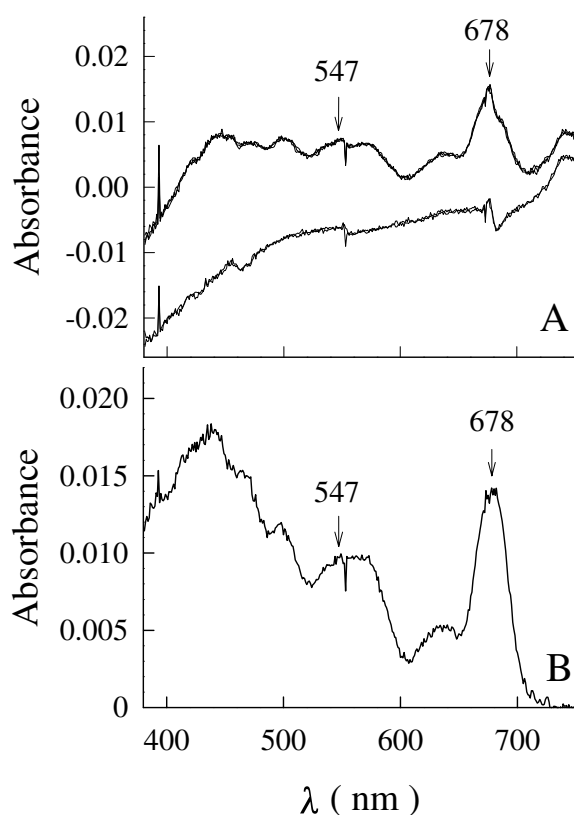


Figure 2. Example of absorbance acquisition obtained with the automated spectrophotometer. A: 2 reference (filtered culture) and 3 culture spectra. B: final spectra based on difference between the averaged culture and reference spectra. Vertical arrows indicate maximum absorbance in the green and red part of the spectrum due to PE and Chl *a*. Peaks at 393 nm, 553 nm and 673 nm are inherent to the spectrophotometer functioning.

dual beam spectrophotometer equipped with an integrating sphere. Measurements were made in the spectral region between $\lambda = 380$ nm and $\lambda = 750$ nm at 1-nm intervals. For each spectral acquisition, filtered (Gelman Filter Type A/E) medium from the cultures were used as reference. The cell suspensions were 'optically thin' enough to ensure that multiple interactions between photons and cells were negligible. Triplicate absorption scans for each sample were reproducible (3.5%) and were averaged to produce the final spectra (Figure 2). To correct the measured absorption spectra for scattering loss, absorbance at 750 nm was subtracted from measurements at all wavelengths.

Determinations of particulate carbon, nitrogen and Chl *a*

Methods for CHN measurements of particulate carbon and nitrogen, and for HPLC estimation of Chl *a* are described in Stramski et al. (2002). Chl *a* (and Chl *c*₂) was also estimated using the spectrophotometric equations of Jeffrey and Humphrey (1975). Filters were ground in 7 mL 90% acetone and left to extract over 12 h at 4 °C. After clarification by centrifugation (3000 × g, 15 min.), corrected spectra of the pigment solution (1-cm quartz cuvette) were recorded on the same spectrophotometer as for the *in vivo* absorption (with 90% acetone as reference).

Sampling for the HPLC and spectrophotometric determinations of Chl *a* was performed at the same time as the *in vivo* absorption measurements.

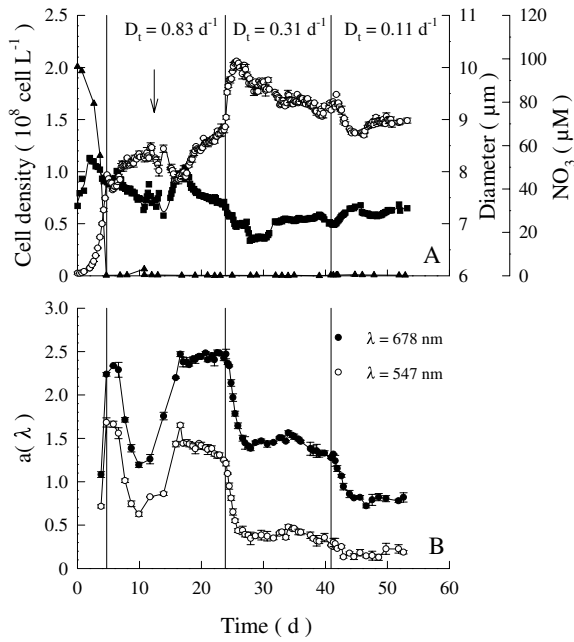


Figure 3. Culture grown at $93 \mu\text{mol photon m}^{-2} \text{s}^{-1}$ and different dilution rates D_t . A: time-course of cell density (○), cell diameter (■) and nitrate concentration in the culture (▲) during the batch ($D_t = 0$) and chemostat phases ($n = 3$, SD). At time 11.64 d (vertical arrow), the inflowing pump of new medium was accidentally stopped for 3 h, preventing the culture from rapidly reaching its equilibrium due to a transient nutrient deprivation. On day 22, the dilution rate was decreased from 0.83 to 0.31 day⁻¹, before the culture had reached complete equilibrium. B: time-course of *in vivo* absorption measured at 678 nm (●) and 547 nm (○) during the different dilution phases D_t . Only two acquisitions were performed during the batch phase, because no renewal could compensate the loss of culture volume due to sampling.

Determination of [Chl *a*] and [PE] from *in vivo* absorption and mean cell size

The specific absorption coefficient of a substance in solution at the wavelength λ , $a_{\text{sol}}^*(\lambda)$, is defined as the ratio of its absorption coefficient $a_{\text{sol}}(\lambda)$ to its concentration [S]:

$$a_{\text{sol}}^*(\lambda) = \frac{a_{\text{sol}}(\lambda)}{[S]} \quad (1)$$

In a phytoplanktonic culture, Chl *a* is not in solution, but subdivided among cells in suspension. The consequence of this packaging is that the *in vivo* absorption $a(\lambda)$ actually measured in the red (at $\lambda = 676$ nm, Chl *a* is the major cellular absorbing component) is lower than $a_{\text{sol}}(\lambda)$, the absorption of the same amount of Chl *a* extracted in solution, and thus cannot serve to estimate directly its concentration [S]. $a(\lambda)$ and $a_{\text{sol}}(\lambda)$ are linked by a factor $Q_a^*(\lambda)$ that has been demonstrated, theoretically, for spherical particles:

$$Q_a^*(\lambda) = \frac{a(\lambda)}{a_{\text{sol}}(\lambda)} \quad (2)$$

Details of the theory and its applicability to phytoplankton particles are given by Morel & Bricaud (1981). The calculation of $a_{\text{sol}}(\lambda)$ requires the determination of the *in vivo* absorption $a(\lambda)$, the cell concentration n_t , and the mean cell diameter d . The calculation of [S] requires, furthermore, $a_{\text{sol}}^*(\lambda)$. $a_{\text{sol}}^*(\text{Chl } a)$ and $a_{\text{sol}}^*(\text{PE})$ are the specific absorption coefficients of Chl *a* extracted in acetone ($0.0206 \text{ m}^2 \text{ mg}^{-1}$, according to SCOR-UNESCO equations), and PE extracted in phosphate buffer ($0.0029 \text{ m}^2 \text{ mg}^{-1}$ (MacColl et al. 1976), respectively).

Growth rate

The cell division rate μ_n was calculated from the time variations of the smoothed cell density (Savitzky-Golay spline estimation, Table Curve 2d v5):

$$\mu_n = \left(\frac{1}{x_n} \right) \times \left(\frac{\Delta X_n}{\Delta t} \right) + D_t \quad (3)$$

where x_n is the smoothed cell number and D_t the dilution rate at time t . The significance of symbols used in the text are given at the end of the discussion.

Results

Growth and cell properties in chemostats renewed with different dilution rates

The automated acquisition shows the changes with time in cell number and size in the chemostat culture (Figure 3A), and reveals unexpected features. For instance, equilibrium had not been reached completely after several days with an unchanged dilution rate of 0.83 day⁻¹, when the cell concentration and size presented small, but significant daily increases of about 4%. Note that cell biovolume, a good proxy of algal biomass, is quite constant during this period (daily variation less than 1%, data not shown), because it integrates the opposite trends in cell size and concentration.

The higher cell density observed after the step decrease of D_t (from 0.81 to 0.31 day⁻¹) fits with chemostat theory which predicts that a stabilized cell density in continuous cultures increases as the dilution is lowered. The transient phase that occurred before the culture stabilization is commonly observed in highly sampled phytoplanktonic cultures. It is easily explained by a temporary mismatch between the

nutrient dependent growth rate and the dilution rate, and by the fact that the limiting nutrient cell quota is responsible for a time delay in the system response to external perturbation.

The second step decrease of the dilution rate (from 0.31 to 0.11 day⁻¹) caused an unexpected decrease in cell density, which contradicts the chemostat theory. In practice, this situation has been observed in continuous cultures at low dilution rates. It has been experimentally demonstrated that, when the renewal rate of new medium per cell is too low (typically this occurs when the dilution rate is low and/or the concentration of the limiting nutrient in the renewal medium is high), phytoplanktonic cultures do not behave strictly as an open system. In consequence, the equilibria observed at low dilution rates did not match with those calculated by the theory (Sciandra & Ramani, 1994). The relatively low level of cell density observed at $D_t = 0.11$ compared to $D_t = 0.31$ day⁻¹ is probably attributable to this phenomenon.

The mean cell diameter ranged between 6.7 and 8.3 μm during this experiment, and, similarly to the cell concentration, displayed small variations at fixed D_t . The lower cell diameter corresponded to the intermediate growth rate of 0.31 day⁻¹, suggesting a curvilinear relationship between growth rate and cell size. The higher cell size measured in the last dilution phase compared to the previous one may also result from the unexpected inverted equilibria of cell density mentioned above.

The high frequency of cell counting allowed us to calculate the cell division rate μ_n at any time from adequate smoothing performed on the cell number series (Figure 4A). The mean division rate calculated during the batch mode in nutrient replete condition was 0.95 day⁻¹. Thereafter, and due to the fact that cell density was not completely stabilized, the mean value of μ_n (0.83 day⁻¹) was slightly greater than the dilution rate (0.81 day⁻¹). For the two other dilution rates (0.31 and 0.11 day⁻¹), μ_n fluctuated around values very similar to D_t (respectively 0.31 and 0.12 day⁻¹). These small fluctuations, which are visible thanks to the high frequency acquisition of cell distribution, are difficult to explain. In any case, the mean growth rates reached at the end of the subsequent dilution phases can be considered as being significantly different from each other, even if an absolute steady state was not completely reached in each phase.

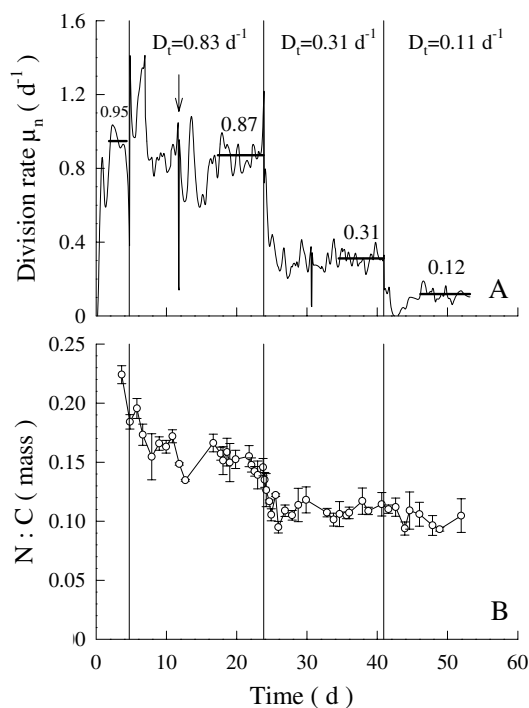


Figure 4. A: time-course of the division rate μ_n . Horizontal bars and attached numbers give the mean division rates calculated at the end of each dilution phase D_t . Average values for the cell quotas and ratios shown in Table 3 are calculated over the interval marked by the horizontal bars. The vertical arrow indicates the time where the inflowing pump was accidentally arrested. B: time-course of the N:C ratio. The observed transient depletion of the N:C ratio observed at day 12 resulted from the temporary arrest of the inflowing pump.

The cell composition and optical properties at the end of the dilution phases can thus be considered as representative of different nitrogen-limited growth levels. As a consequence of the increasing levels of nitrogen limitation driven by the successive decreasing dilution rates, the N:C ratio decreased with time (Figure 4B). The *in vivo* absorption measured in the red and green parts of the spectrum (Figure 3B) showed considerable variations which, interestingly, are not correlated with the cell concentration. Because particulate absorption measured at 678 nm is essentially due to Chl *a*, the variations of $a(678)$ reflect those of the cell density and optical cross-section for absorption, the latter being principally dependant on Chl *a_i*, the internal cell concentration of Chl *a*, and cell size. Consequently, the absorption signal, being completely different from the cell concentration evolution, is thus principally driven by Chl *a_i*.

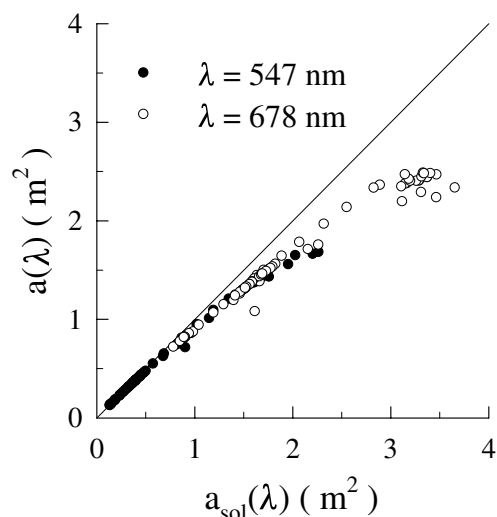


Figure 5. Comparison of $a_{\text{sol}}(\lambda)$ and $a(\lambda)$ at 678 (●) and 547 nm (○).

Estimation of [Chl *a*] and [PE] from *in vivo* absorption measurements

Figure 5 shows the relationships existing between $a(\lambda)$ and $a_{\text{sol}}(\lambda)$, measured at the peaks of Chl *a* in the red ($\lambda = 678$) and of PE in the green ($\lambda = 547$ nm) respectively. The data points ($n = 72$) were acquired during the studies shown in Figure 3 and cover a wide range of nitrogen limitation. The curvilinear shape reflects the flattening effect due to pigments being concentrated inside cells.

The suitability of *in vivo* absorption measurements to estimate Chl *a* in phytoplanktonic cultures can be verified by comparing the calculated values with the concentration actually measured by HPLC or spectrophotometric methods. Table 2 summarizes the experimental conditions from 9 continuous cultures during which absorption measurements at 678 nm were performed simultaneously with HPLC and spectrophotometric determinations of [Chl *a*]. Figures 6a and b shows that [Chl *a*] calculated from *in vivo* absorption is a very good proxy of both [Chl *a*] measured either by HPLC ($r^2 = 0.96$, $n = 85$, slope = 0.9436) or spectrophotometric equations ($r^2 = 0.94$, $n = 78$, slope = 1.0728).

Since we were unable to extract PE efficiently for spectrophotometry, [PE] was estimated from *in vivo* absorption at 547 nm corrected for the packaging effect. Nitrogen limitation has a considerable effect on the Chl *a*:C (θ) and PE:C ratios (Figure 7). Examination of cell quota (Table 3) reveals that the variation of these ratios is partly due to an increase of C per

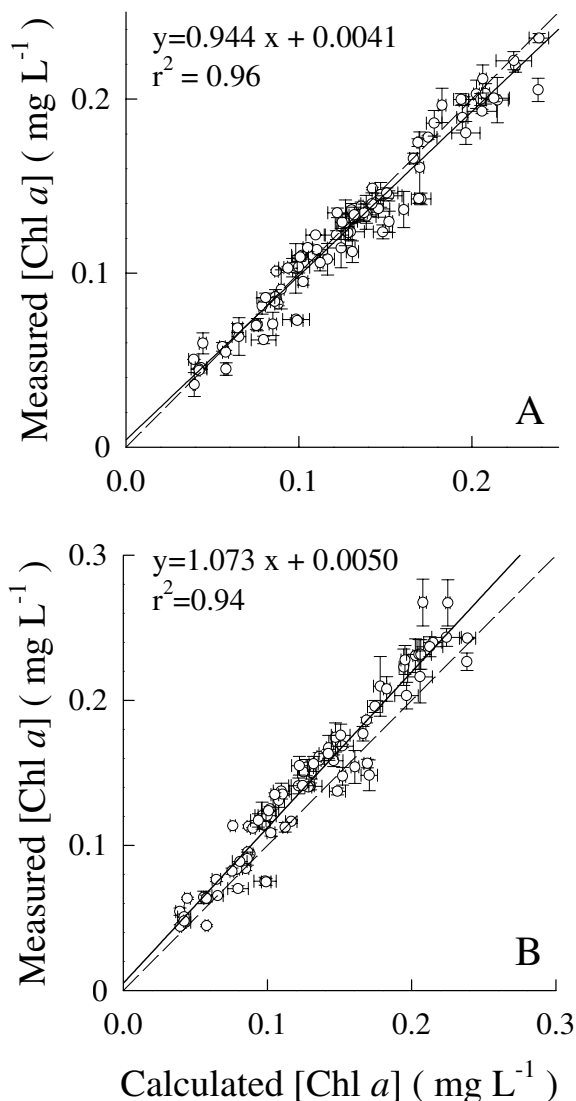


Figure 6. Comparison of Chl *a* concentration measured by HPLC (A) or spectrophotometer (B) with Chl *a* concentration calculated from *in vivo* absorption at 678 nm. Data were acquired under a range of light and nitrogen conditions (see Table 2).

cell. However, the data also show that the intracellular concentration of Chl *a* decreases with the level of N limitation and contributes significantly to the variation in θ . The amplitude of change in the PE pool is much more important than for the Chl *a* pool: between $D_t = 0.83$ and $D_t = 0.31 \text{ day}^{-1}$, PE:C decreases by a factor 5.6, while θ decreases only 2.8.

Table 2. PAR ($\mu\text{mol photon m}^{-2} \text{s}^{-1}$), $[\text{NO}_3]$ in the renewal medium (μM), dilution rate D_t (day^{-1}) and temperature ($T^\circ\text{C}$) conditions during *in vivo* absorption acquisitions and samplings for extracted Chl *a* measurements (HPLC and spectrophotometric methods)

PAR	12 ± 1	15 ± 2	15 ± 1	17 ± 1	29 ± 1	30 ± 3	93 ± 11	95 ± 10	313 ± 21
									0.00
D_t	0.00	0.00	0.00	0.00	0.00	0.00	0.83 ± 0.09	0.50 ± 0.05	0.69 ± 0.02
	0.11 ± 0.01	0.21 ± 0.02	0.21 ± 0.02	0.11 ± 0.01	0.19 ± 0.01	0.09 ± 0.00	0.31 ± 0.01	0.10 ± 0.00	0.49 ± 0.04
							0.11 ± 0.00	0.80 ± 0.03	0.33 ± 0.04
									0.12 ± 0.00
$[\text{NO}_3]$	91 ± 4	91 ± 4	43 ± 2	43 ± 2	40 ± 2	40 ± 2	96 ± 14	96 ± 14	169 ± 4
$T^\circ\text{C}$	19 ± 0.5	19 ± 0.5	19 ± 0.5	19 ± 0.5	19 ± 0.5	19 ± 0.5	19 ± 0.5	19 ± 0.5	19 ± 0.5

Table 3. Average values of the mean division rate μ_n (day^{-1}), cell content of C, N, Chl *a*, and PE (pg cell^{-1}), and N:C, Chl *a*:C, PE:C ratios (g/g) measured at different dilution rates D_t (day^{-1}) in a continuous culture of *Rhodomonas salina* ($93 \pm 11 \mu\text{mol photon m}^{-2} \text{s}^{-1}$)

D_t	μ_n	Cell C	Cell N	Cell Chl <i>a</i>	Cell PE	N:C	Chl <i>a</i> :C	PE:C
0	0.95							
0.83	0.87 ± 0.07	57.80 ± 3.59	8.63 ± 0.62	1.21 ± 0.06	4.01 ± 0.35	0.153 ± 0.003	0.0201 ± 0.0004	0.0743 ± 0.0028
0.31	0.31 ± 0.04	63.50 ± 2.54	6.85 ± 0.37	0.48 ± 0.03	0.82 ± 0.13	0.109 ± 0.002	0.0075 ± 0.0003	0.0133 ± 0.0009
0.11	0.12 ± 0.02	65.30 ± 2.04	6.57 ± 0.75	0.28 ± 0.01	0.45 ± 0.11	0.104 ± 0.008	0.0044 ± 0.0003	0.0062 ± 0.0008

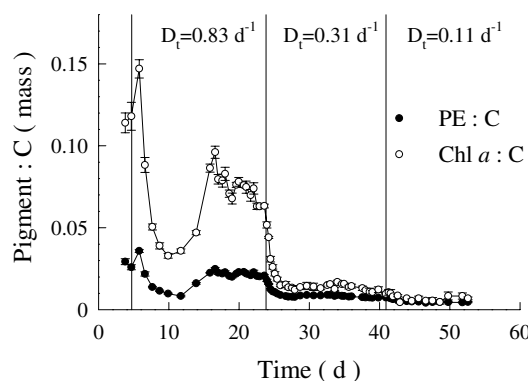


Figure 7. Time-course of Chl *a*:C (●) versus PE:C (○) ratio during the different dilution phases D_t .

Discussion

Automatic acquisition of *in vivo* absorption

Our system measures automatically (besides cell size and numbers, NO_3 and NO_2 concentrations) the spectral absorption of *in vivo* phytoplankton cultures with good reproducibility (Figure 2). The only necessary technical intervention is the regular replacement of filters and rinsing solutions. As the reference and culture

absorption spectra are successively acquired within the same flow cell, the system is quite insensitive to an eventual long term cuvette fouling. Brij doubles as a detergent and wetting agent, thus preventing air bubble accumulation on the cuvette walls. However, Brij requires adequate rinsing procedure, so the operating cycle length (nearly 30 min) and the amount of culture volume required for each measurement. This can limit the frequency of data acquisition, particularly in continuous cultures maintained at low dilution rates, where the sampling volume may exceed the culture renewal.

Despite the fact that two independent measurements (absorption and size spectra) are required to estimate $[\text{Chl } a]$ optically, this method presents real advantages compared to HPLC and spectrophotometry. The most obvious is the reduced cost and simplicity. With the same spectra acquisition, it is possible to determine the concentration of at least 2 different pigments (in this work: Chl *a* and PE), whereas their traditional estimations require 2 separate extractions of 2 different filters in 2 different solvents.

Estimating pigment concentration from in vivo absorption and mean cell diameter

The optical method is based on the assumption of the anomalous diffraction approximation (Van de Hulst 1957). The equations were developed as an extension of the Mie theory on particles in suspension which 1) are spherical, 2) are homogeneous, and 3) have a refractive index differing only slightly from the surrounding medium. Morel and Bricaud (1986) demonstrated that the phytoplankton refractive index generally fulfilled the latter condition. Contrary to the second tenet, algal cells are diverse in shape and size, which undergo variations in their intracellular composition and present a heterogeneous distribution of their internal pigments and other components. The internal packaging of pigments in the chloroplasts may influence cellular optical properties (Berner et al. 1989). Despite this apparent complicated optical system compared to the theoretical simplifying assumptions, Bricaud et al. (1988) successfully applied the Van de Hulst model to nine species of phytoplankton from diverse classes. As demonstrated by the results obtained with an ovoid species, *Cryptomonas* sp. (Sciandra et al. 2000), *Rhodomonas salina* (this study), and the cylindrical species, *Thalassiosira pseudonana* (Stramski et al. 2002), deviations from an ideal sphere can be supported to some extent. This method could be thus be applied routinely, at least for Chl *a*, which is present in all the microalgae. For classes which also contain Chl *b*, absorption should overlap at 678 nm with Chl *a* and would be taken into account. The cell concentration must be sufficient to generate an *in vivo* spectrophotometric signal significantly different from the reference signal (Figure 2). However, the cell density must not exceed an upper limit for which the suspension cannot be considered as optically thin (Morel and Bricaud 1981).

Figure 6a shows that the optical and HPLC methods give comparable measures of [Chl *a*]. As the HPLC method is calibrated by measuring the absorption of different concentrated Chl *a* standards extracted in acetone, [Chl *a*] estimated by this method is independent from the specific absorption coefficient $a_{\text{Chl}a}^*$. This is not the case for the optical approach, in which $a_{\text{sol}}(678)$ is divided by $a_{\text{Chl}a}^*$ to determine Chl a_i . The value of $0.0206 \text{ m}^2 \text{ mg}^{-1}$ used was originally determined at 663 nm for Chl *a* dissolved in 90% acetone, so it is uncertain whether it is the same for Chl *a* in cytoplasm. Alternate approaches which have studied *in vivo* absorption spectra of intact pigment-

protein complexes show that the maximum unpacked absorption at 675 nm is higher than the red peak value in acetone i.e. near $0.027 \text{ m}^2 \text{ mg}^{-1}$ Chl *a* according to Johnson et al. (1994). The good agreement between the HPLC and optical methods suggests that the value of $a_{\text{Chl}a}^*$ used in this study to calculate Chl a_i from $a_{\text{sol}}(678)$ is appropriate, and that this value does not differ markedly according to whether Chl *a* is dissolved in acetone or in cell cytoplasm.

Relationships between nitrogen status, absorption, cell concentration and cell quota

Absorption and fluorescence are bulk optical properties currently used to estimate phytoplankton biomass. Our results show that absorption measured in the red part of the spectrum is not necessarily a good proxy of the phytoplankton population (Figure 3), because of a discrepancy between absorption and cell number due to the plasticity of the Chl *a* pool under nitrogen deficiency (see Table 3). It is interesting to note that equilibria of Chl *a* and cell concentrations have opposite trends when the dilution rate is increased in continuous cultures. The higher concentrations of Chl *a* reached in more diluted cultures indicates that the negative effect of dilution on cell concentration is largely compensated by an increase of internal Chl *a*, triggered by more available nitrogen which is used to sustain higher carbon fixation and growth rate.

A second source of discrepancy between cell population and absorption is inherent in the fact that the same concentration of chlorophyll in the sea water does not produce the same absorbance at 678 nm, depending on its distribution among particles. The packaging of Chl *a* into discrete cells induces a non-linear flattening of the absorption response, which increases with cell size and internal chlorophyll concentration. In consequence, the growth conditions also influence the flattening effect, and consequently, the non-linearity between chlorophyll concentration and absorbance.

Our results show that θ , the ratio of Chl *a* to C, which is well known to respond to variations in light intensity, is also very sensitive to the nitrogen status at fixed PAR (Figure 7). The reduction of θ , under nitrogen limitation reflects primarily a reduction of the Chl *a* per cell, which can be interpreted following two different hypothetical processes. First, to recover a balanced growth under nitrogen limitation, cells reduce the rate of photosynthesis by decreasing the rate of photon absorption. Secondly, the breakdown of

apoproteins included in the light harvesting complexes is a source of nitrogen usable in case of deprivation. The larger amplitude of variation observed for the PE content relative to chlorophyll suggests that these two pigments are differently affected by the nitrogen status. PE is an accessory pigment which transfers the absorbed energy to the PSII of Chl *a* and does not intervene directly in carbon fixation. Moreover, functional phycobiliproteins contain large amounts of nitrogen. This may explain why PE is mobilized more than Chl *a* under nitrogen deficiency.

Acknowledgements

We thank Joséphine Ras for technical help in HPLC measurements and Patrick Chang for improving the English. We also thank Annick Bricaud and the anonymous reviewers for their valuable comments. This research was supported by PROSOPE program (CNRS).

Nomenclature

Symbol	Significance	Units
λ	Light wavelength	nm
μ_n	Cell division rate	day ⁻¹
$a(\lambda)$	Absorption coefficient of cell suspension	m ⁻¹
$a_{sol}(\lambda)$	Absorption coefficient of substance ideally dispersed into solution	m ⁻¹
$a^*_{sol}(\lambda)$	Specific absorption coefficient of substance	m ² mg ⁻¹
$a^*_{sol}(\text{Chl } a)$	Specific absorption coefficient of Chl <i>a</i> (extracted in 90% acetone)	m ² mg ⁻¹
$a^*_{sol}(\text{PE})$	Specific absorption coefficient of PE (extracted in phosphate buffer)	m ² mg ⁻¹
Chl a_i	Cellular Chl <i>a</i> concentration	$\mu\text{g mm}^{-3}$
[Chl <i>a</i>]	Chl <i>a</i> concentration in the culture	mg L ⁻¹
θ	Mass ratio of Chl <i>a</i> to C	dimensionless
d	Cell diameter	μm
D_t	Dilution rate	day ⁻¹
N:C	Mass ratio of N to C	dimensionless
n_t	Cell abundance at time <i>t</i>	cells L ⁻¹
PAR	Photosynthetically available radiation	$\mu\text{mol photon m}^{-2} \text{ s}^{-1}$
PE _{<i>i</i>}	Cellular PE concentration	$\mu\text{g mm}^{-3}$
[PE]	PE concentration in culture	mg L ⁻¹
$Q_a^*(\lambda)$	Factor of spectral flattening	dimensionless
[S]	S concentration in culture	g m ⁻³
x_n	Smoothed cell number	cells L ⁻¹

References

- Anning T, MacIntyre H.L., Pratt S.M., Sammes P.J., Gibb S. and Geider R.J. 2000. Photoacclimation in the marine diatom *Skeletonema costatum*. *Limnol. Oceanogr.* 45: 1807–1817.
- Berges J.A., Charlebois D.O., Mauzerall D.C. and Falkowski P.G. 1996. Differential effects of nitrogen limitation on photosynthetic efficiency of photosystems I and II in microalgae. *Plant Physiol.* 110: 689–696.
- Bernard O., Malara G. and Sciandra A. 1996. The effects of a controlled fluctuating nutrient environment on continuous cultures of phytoplankton monitored by a computer. *J. exp. mar. Biol. Ecol.* 197: 263–278.
- Berner T., Dubinsky Z., Wyman K. and Falkowski P.G. 1989. Photoacclimation and the 'package' effect in *Dunaliella tertiolecta* (Chlorophyceae). *J. Phycol.* 25: 70–78.
- Bricaud A., Bedhomme A.L. and Morel A. 1988. Optical properties of diverse phytoplanktonic species: Experimental results and theoretical interpretation. *J. Plankton Res.* 10: 851–873.
- Dubinsky Z. 1992. The functional and optical absorption cross-sections of phytoplankton photosynthesis. In Falkowski P.G., Woodhead A.D. (eds), *Primary Productivity and Biogeochemical Cycles in the Sea*, Plenum Press, New York, pp. 31–45.
- Duysens L.M.N. 1956. The flattening effect of the absorption spectra of suspensions as compared to that of solutions. *Biochem. biophys. Acta* 19: 1–12.
- Flynn K.J., Marshall H. and Geider R.J. 2001. A comparison of two N-irradiance interaction models of phytoplankton growth. *Limnol. Oceanogr.* 46: 1794–1802.
- Geider R.J., MacIntyre H.L. and Kana T.M. 1998. A dynamic regulatory model of phytoplanktonic acclimation to light, nutrients, and temperature. *Limnol. Oceanogr.* 43: 679–694.

- Goericke R. and Montoya J.P. 1998. Estimating the contribution of microalgal taxa to chlorophyll a in the field – variations of pigment ratios under nutrient- and light-limited growth. *Mar. Ecol. Progr. Ser.* 169: 97–112.
- Healey F.P. 1985. Interacting effects of light and nutrient limitation on the growth rate of *Synechococcus linearis* (Cyanophyceae). *J. Phycol.* 21: 134–146.
- Jeffrey S.W. and Humphrey G.F. 1975. New spectroscopic equations for determining Chlorophylls a, b, c1 and c2 in higher plants, algae and natural phytoplankton. *Biochem. Physiol. Pflanzen* 167: 191–194.
- Johnsen G., Nelson N.B., Jovine, R.V.M. and Prezelin, B.B. 1994. Chromoprotein- and pigment-dependent modelling of spectral light absorption in two dinoflagellates, *Prorocentrum minimum* and *Heterocapsa pygmaea*. *Mar. Ecol. Progr. Ser.* 114: 245–258.
- Kana T.M., Feiwel N.L. and Flynn L.C. 1992. Nitrogen starvation in marine *Synechococcus* strains: clonal differences in phycobiliprotein breakdown and energy coupling. *Mar. Ecol. Progr. Ser.* 88: 75–82.
- MacColl R., Berns D.S. and Gibbons O. 1976. Characterization of cryptomonad phycoerythrin and phycocyanin. *Arch. Biochem. Biophys.* 177: 265–275.
- Malara G. and Sciandra A. 1991. A multiparameter phytoplanktonic culture system driven by microcomputer. *J. appl. Phycol.* 3: 235–241.
- Morel A. and Bricaud A. 1981. Theoretical results concerning light absorption in a discrete medium, and application to specific absorption of phytoplankton. *Deep-Sea Res.* 28A: 1375–1393.
- Morel A. and Bricaud A. 1986. Inherent optical properties of algal cells including picoplankton: theoretical and experimental results. *Can. Bull. Fish. aquat. Sci.* 214: 521–559.
- Pawlowski L., Bernard O., Le Floc'h E. and Sciandra A. (in press) Qualitative behaviour of phytoplankton growth model in photobioreactor. In 15th IFAC World Congress, Barcelona, Spain, July 2002.
- Rhee G.Y. and Gotham I.J. 1981. The effect of environmental factors on phytoplankton growth: light and the interactions of light with nitrate limitation. *Limnol. Oceanogr.* 26: 649–659.
- Sciandra A., Gostan J., Collos Y., Descolas-Gros C., Leboulanger C., Martin-Jézéquel V., Denis M., Lefèvre D., Copin-Montégut C. and Avril B. 1997. Growth compensating phenomena in continuous cultures of *Dunaliella tertiolecta* limited simultaneously by light and nitrate. *Limnol. Oceanogr.* 42: 1325–1339.
- Sciandra A., Lazzara L., Claustre H. and Babin M. 2000. Responses of the growth rate, pigment composition and optical properties of *Cryptomonas* sp. to light and nitrogen stresses. *Mar. Ecol. Progr. Ser.* 201: 107–120.
- Sciandra A. and Ramani P. 1994. The steady states of continuous cultures with low rates of medium renewal per cell. *J. exp. mar. Biol. Ecol.* 178: 1–15.
- Stramski D., Sciandra A. and Claustre H. 2002. Effects of temperature, nitrogen, and light limitation on the optical properties of the marine diatom *Thalassiosira pseudonana*. *Limnol. Oceanogr.* 47: 392–403.
- Turpin D.H. 1991. Effects of inorganic N availability on algal photosynthesis and carbon metabolism. *J. Phycol.* 27: 14–20.
- Van de Hulst H.C. 1957. *Light Scattering by Small Particles*, Wiley, New York, 470 pp.